⟨G|QC|J⟩

OUTLINE

Implementing Unitary Coupled Cluster On a Quantum Computer†

Oskar Grzegorowski*[a]

The scaling of classical Unitary Coupled Cluster remains to be one of the biggest hindrances holding the theory back, however its implementations on quantum computers have the potential to solve this issue, and elevate the theory beyond its current limits. That said, to many the construction of UCC ansätze within quantum circuits, and the processes surrounding their applications, remain ambiguous. In this outline we provide an in depth exploration of UCC ansätze and their implementation on quantum computers. We introduce variations of UCC designed specifically with quantum circuits in mind, notably k-UpCCGSD, and compare the performance of their implementations run on both ideal, and currently available noisy quantum devices. Our findings demonstrate that in theory quantum computing can enhance UCC capabilities, however its practical implementations are held back by the severe limitations of modern quantum computers.

1 Introduction

Quantum computing remains to be one of the most promising ways of advancing the way we understand and simulate molecular systems. In theory, it should allow us to go beyond the scope of classical machines, and develop new innovative tools which open up new avenues in the field of computational quantum chemistry. Due to their quantum nature, quantum computers excel in many areas where classical computers struggle, such as simulating quantum systems or solving certain types of optimization problems. Among the various quantum inspired approaches, the application of quantum computing principles into Unitary Coupled Cluster Theory stands out as a compelling approach to advancing the accuracy and efficiency of CC calculations.

Coupled Cluster Theory stands as a powerful and widely used method for accurately describing the structure and properties of many-body systems. However, the traditional classical implementations of UCC are often hindered by their exponential scaling with system size, which renders its application to larger molecules limited. Quantum computers have the potential to handle larger systems more efficiently, allowing UCC to tackle problems currently beyond the reach of classical CC.

It is however important to note, that while in theory a quantum implementation of UCC has the capacity to outperform its classical counterpart, it would require accurate and robust hardware to operate on. Current quantum computers have made significant strides in terms of their capabilities, but they still face challenges in terms of accuracy. They are highly sensitive devices, extremely prone to noise and errors, which leads to calculational inaccuracies.

2 Theory

2.1 Coupled Cluster Theory

In quantum chemistry Coupled Cluster (CC)[1] is a post Hartree-Fock method used to describe the electronic structure of many body systems. It has been used to compute relatively accurate approximations of various molecular properties while being less computationally demanding than methods such as FCI (Full Configuration Interaction). The CC wavefunction is given by a series of excitation operators acting on a reference state, typically a Slater determinant constructed from Hartree-Fock orbitals:

$$|\Psi_{\mathrm{CC}}\rangle = e^{\hat{\mathrm{T}}}|\Phi_{\mathrm{ref}}\rangle \tag{1}$$

here $|\Phi_{\mathrm{ref}}\rangle$ is the HF reference state, and operator $\hat{\mathrm{T}}$ is the cluster operator. The choice of cluster operator, in conjunction with a strategy for determining the optimal amplitudes described below, defines a given method, and the general form of the state created by the application of the cluster operator is called an ansatz. If this operator consists of fermionic excitations from occupied to virtual orbitals, the generated ansatz is referred to as traditional coupled-cluster (TCC), and its exponential map is given by its Taylor expansion:

$$\hat{\mathrm{T}} = \sum_{k=1}^{n} \hat{\mathrm{T}}_k \tag{2}$$

[a] Corresponding author: Oskar.Grzegorowski@UGent.be

$$\hat{\mathrm{T}}_k = \frac{1}{(k!)^2} \sum_{\substack{i,j,\ldots \\ a,b,\ldots}} t_{ij\ldots}^{ab\ldots} \hat{\mathrm{a}}_a^\dagger \hat{\mathrm{a}}_b^\dagger \ldots \hat{\mathrm{a}}_j \hat{\mathrm{a}}_i \tag{3}$$

here each $\hat{\mathrm{T}}_n$ consists of k annihilation and k creation operators acting on occupied and virtual orbitals in the reference state respectively. The choice of different values of n yields different truncated ansätze. If n equals the number of electrons, the FCI wave function lies within the manifold of wavefunctions represented by the TCC wave function and no approximation is made. Comparing the exact CC solution with full CI, where each $\hat{C}_i$ is the operator which generates all i-fold configuration terms, it can be shown that[2]:

$$\hat{C}_1 = \hat{T}_1 \tag{4}$$

$$\hat{C}_2 = \hat{T}_2 + \frac{1}{2}\hat{T}_1^2 \tag{5}$$

$$\hat{C}_3 = \hat{T}_3 + \hat{T}_1\hat{T}_2 + \frac{1}{3!}\hat{T}_1^3 \tag{6}$$

$$\hat{C}_4 = \hat{T}_4 + \frac{1}{2}\hat{T}_2^2 + \hat{T}_1\hat{T}_3 + \frac{1}{2}\hat{T}_1^2\hat{T}_2 + \frac{1}{4!}\hat{T}_1^3 \tag{7}$$

In these decompositions it can be seen that for a given i-fold configuration term, all $\hat{T}_j$ terms for $j \leq i$ are contributing to the expression for the operator. Hence for example, a coupled-cluster wave function limited to only double excitations already includes the disconnected parts of quadruples, hextuples, and higher even ordered excitations. This implicit connection to all higher order configurations grants truncated CC and its variations a considerable degree of accuracy, out-performing essentially all other standard single-reference methods with comparable computational cost.

2.2 Basics of Quantum Computing

This section contains the basics of quantum computing theory necessary for understanding the contents of this outline. In quantum computing (QC)[3] quantum-mechanical phenomena such as superposition and entanglement, are used to process information. In QC, the basic unit of information is the qubit, which, unlike classical bits, which have to be in state 0 or 1, can exist in a superposition, a linear combination of states with complex coefficients or amplitudes. The modulus square of each amplitude is the probability of the corresponding state being observed, and the sum of the modulus square of all possible states must equal to 1. This result is known as the Born's rule. For a two-level qubit defined in the orthonormal basis, state 0 or 1 can be represented as unit vectors:

$$|0\rangle = \begin{pmatrix} 1 \\ 0 \end{pmatrix} \quad \text{and} \quad |1\rangle = \begin{pmatrix} 0 \\ 1 \end{pmatrix} \tag{8}$$

In this instance the superposition between the two states can be represented as:

$$|\Psi\rangle = \alpha|0\rangle + \beta|1\rangle, \quad \text{where } \alpha, \beta \in \mathbb{C} \tag{9}$$

In quantum mechanics an operator is unitary if its Hermitian conjugate is equal to its inverse:

$$\hat{U}^\dagger = \hat{U}^{-1} \tag{10}$$

and the operator multiplied by its Hermitian conjugate gives the identity operator:

$$\hat{U}^\dagger \cdot \hat{U} = \hat{U} \cdot \hat{U}^\dagger = \hat{I} \tag{11}$$

In QC it is necessary that any operators acting on qubits are unitary. When an operation is applied to a quantum state, the probabilities of different measurement outcomes should still add up to 1 (the sum of the modulus square of all possible states must equal to 1). Unitary operators ensure that the total probability remains conserved. Another reason is that unitary operators are reversible, meaning that they can be applied in both the forward and backward directions, which allows for manipulation and transformation of quantum states without losing any information. In quantum computing, unitary operators can be represented as matrices, and they are commonly referred to as gates. Unitary gates acting on qubits are fundamental building blocks in quantum circuits. Here is a short list of fundamental quantum gates used in this outline:
Pauli matrices:

$$\begin{aligned} \sigma_0 \equiv I = \begin{pmatrix} 1 & 0 \\ 0 & 1 \end{pmatrix} \qquad \sigma_1 \equiv \sigma_x \equiv X = \begin{pmatrix} 0 & 1 \\ 1 & 0 \end{pmatrix} \\ \sigma_2 \equiv \sigma_y \equiv Y = \begin{pmatrix} 0 & -i \\ i & 0 \end{pmatrix} \qquad \sigma_3 \equiv \sigma_z \equiv Z = \begin{pmatrix} 1 & 0 \\ 0 & -1 \end{pmatrix} \end{aligned} \tag{12}$$

These gates act on qubits, and allow to reach any point in the geometrical representation called the Bloch sphere fig. 1, where a qubit is represented as a point on a sphere. A commonly adopted convention designates the two antipodal points on the sphere as representatives of the computational basis elements.

The X gate is also called the NOT gate, as it flips the basis set of a qubit ($|0\rangle \rightarrow |1\rangle, \quad |1\rangle \rightarrow |0\rangle$).
The Hadamard gate is one of the most important single qubit gates. It enables to put a qubit from a definite computational basis state into a superposition of the two states:

$$H = \frac{1}{\sqrt{2}} \begin{pmatrix} 1 & 1 \\ 1 & -1 \end{pmatrix} \tag{13}$$

When applied to $|0\rangle$ and $|1\rangle$ it returns:

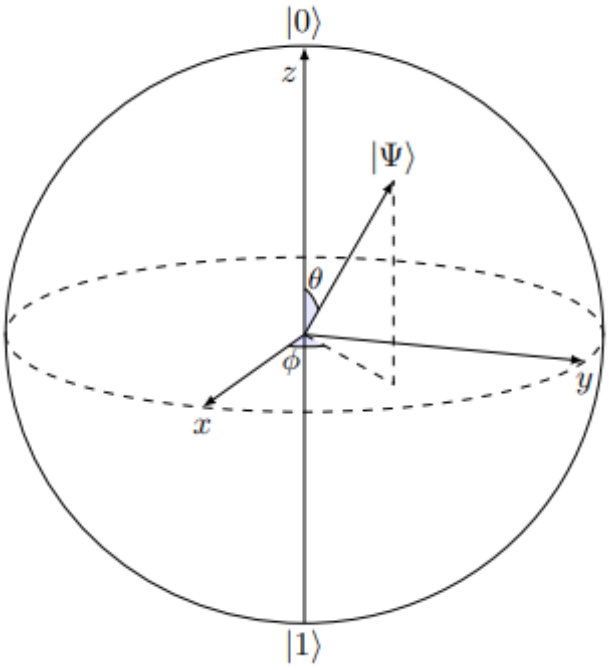

Fig. 1 Taken from:[3]; Exemplary drawing of a block sphere. A Bloch sphere is a geometric representation of the state space of a single qubit in quantum computing, visualizing the possible quantum states as points on a unit sphere. In this example three qubits are shown: qubit $|0\rangle$ is in state 0 (off), qubit $|1\rangle$ is in state 1 (on), and qubit $|\Psi\rangle$ is a superposition between states $|0\rangle$ and $|1\rangle$.

$$H|0\rangle = \frac{1}{\sqrt{2}}\begin{pmatrix}1 & 1\\ 1 & -1\end{pmatrix}\begin{pmatrix}1\\0\end{pmatrix} = \frac{1}{\sqrt{2}}\begin{pmatrix}1\\1\end{pmatrix} = \frac{1}{\sqrt{2}}|0\rangle + \frac{1}{\sqrt{2}}|1\rangle \tag{14}$$

$$H|1\rangle = \frac{1}{\sqrt{2}}\begin{pmatrix}1 & 1\\ 1 & -1\end{pmatrix}\begin{pmatrix}0\\1\end{pmatrix} = \frac{1}{\sqrt{2}}\begin{pmatrix}1\\-1\end{pmatrix} = \frac{1}{\sqrt{2}}|0\rangle - \frac{1}{\sqrt{2}}|1\rangle$$

The total probability of the resulting states (the sum of squares of absolute amplitudes associated with each basis state, or the length of the vector connecting the origin to the point represented by the qubit on a block sphere) is in both cases equal 1, which means that Born's rule is satisfied and if we perform a measurement, there is an equal probability 0.5 of measuring either state $|0\rangle$ or $|1\rangle$. On the block sphere, the Hadamard gate can be understood as a rotation of 180° around the x and z axes.

The $R_x(\theta)$ gate is a gate performing a rotation around the x axis, where θ is the rotation angle:

$$R_x(\theta) = \begin{pmatrix}\cos\frac{\theta}{2} & -i\sin\frac{\theta}{2}\\ -i\sin\frac{\theta}{2} & \cos\frac{\theta}{2}\end{pmatrix} \tag{15}$$

Analogously the $R_z(\theta)$ gate is a gate performing a rotation around the z-axis, where θ is the rotation angle:

$$R_z(\theta) = \begin{pmatrix}e^{-i\frac{\theta}{2}} & 0\\ 0 & e^{i\frac{\theta}{2}}\end{pmatrix} \tag{16}$$

Input	Output
$\|00\rangle$	$\frac{\|00\rangle + \|11\rangle}{\sqrt{2}}$
$\|01\rangle$	$\frac{\|01\rangle + \|10\rangle}{\sqrt{2}}$
$\|10\rangle$	$\frac{\|00\rangle - \|11\rangle}{\sqrt{2}}$
$\|11\rangle$	$\frac{\|01\rangle - \|10\rangle}{\sqrt{2}}$

Fig. 2 Taken from:[3]; The coresponding inputs and outputs on a quantum circuit consisting of a Hadamard gate on the first qubit, and a controlled-NOT gate where the first qubit is the control qubit.

Another main gate, but acting on two qubits, is the controlled-NOT *CNOT* gate, defined as:

$$CNOT = \begin{pmatrix}1 & 0 & 0 & 0\\ 0 & 1 & 0 & 0\\ 0 & 0 & 0 & 1\\ 0 & 0 & 1 & 0\end{pmatrix} \tag{17}$$

This gate is used to entangle two single qubits. Here is an example of a quantum circuit containing a *CNOT* gate [see in a simulator]:

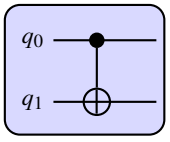

In this example qubit q_0 is the control qubit, and the *NOT* gate is applied to qubit q_1 if q_0 is in the "on" state $|1\rangle$.
In this example a Hadamard gate is applied to q_0, which means that a superposition is applied to the control gate [see in a simulator]:

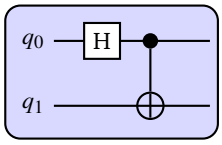

In this case the output on both wires will be a superposition fig. 2. Once qubits are entangled by a *CNOT* gate their states become dependent on each other. The qubits can be disentangled by applying another *CNOT* gate to them.

2.3 Implementing the Unitary Coupled Cluster on a Quantum Computer

Knowing that all operators used in quantum circuits must be unitary, we define Unitary Coupled Cluster[1] (UCC) as a variation on

CC where the cluster operator is of the form $\hat{T} - \hat{T}^\dagger$, then $e^{\hat{T}-\hat{T}^\dagger}$ is unitary. The cluster operator $\hat{T}$ consists of single, double, ..., (up to n-fold) fermionic excitations. On a quantum computer the UCC ansatz is implemented by constructing a unitary operator U defined as such:

$$U = e^{\hat{T}-\hat{T}^\dagger} \tag{18}$$

Where the individual excitation operators are given by:

$$\hat{T} = \sum_i \hat{T}_i \tag{19}$$

here index i goes over all excitations. In UCC the individual excitation operators do not commute with each other which can lead to complex and non-trivial interactions between them. This makes it challenging to implement UCC in a quantum circuit directly. For this reason approximations have to be done using the Trotter decomposition. The first-order decomposition formula is given by:

$$e^{\hat{T}-\hat{T}^\dagger} = e^{\sum_i \theta_i(\hat{T}_i - \hat{T}_i^\dagger)} \approx (\prod_i e^{\frac{\theta_i}{t}(\hat{T}_i - \hat{T}_i^\dagger)})^t + O(\frac{1}{t}) \tag{20}$$

where t is the order of decomposition, also called the Trotter number, and $O(\frac{1}{t})$ is the correction term. θ_i is the amplitude / parameter corresponding to excitation i. Using this formula the parameterized wavefunction can be expressed as:

$$|\Psi_{\mathrm{UCC}}(\theta)\rangle = U|\Phi_{\mathrm{ref}}\rangle = e^{\sum_i \theta_i(\hat{T}_i - \hat{T}_i^\dagger)}|\Phi_{\mathrm{ref}}\rangle \approx \tag{21}$$

$$\prod_i e^{\theta_i(\hat{T}_i - \hat{T}_i^\dagger)}|\Phi_{\mathrm{ref}}\rangle \tag{22}$$

The Trotter decomposition is an approximation, and thus does introduce error, however it is worth noting, that the VQE optimization procedure described later does partially account for the caused error.

When individual $\hat{T}_i$ and $-\hat{T}_i^\dagger$ terms are put together single and double excitations can be given by[4]:

$$\theta(\hat{T}_p^k - (\hat{T}_p^k)^\dagger) \equiv \theta(a_k^\dagger a_p - a_p^\dagger a_k) \quad \textit{and} \tag{23}$$

$$\theta(\hat{T}_{pq}^{kl} - (\hat{T}_{pq}^{kl})^\dagger) \equiv \theta(a_k^\dagger a_l^\dagger a_p a_q - a_p^\dagger a_q^\dagger a_k a_l) \tag{24}$$

Unitary operators performing these excitations are then given by:

$$U_p^k(\theta) = e^{\theta(\hat{T}_p^k - (\hat{T}_p^k)^\dagger)} \quad \textit{and} \tag{25}$$

$$U_{pq}^{kl}(\theta) = e^{\theta(\hat{T}_{pq}^{kl} - (\hat{T}_{pq}^{kl})^\dagger)} \tag{26}$$

These operators can be represented within a quantum circuit by using an encoding such as Jordan-Wigner or Bravyi-Kitaev. Within Jordan-Wigner creation and annihilation operators can be expressed using quantum gates as such:

$$a_p = Q_p \prod_{r=0}^{p-1} Z_r = \frac{1}{2}(X_i + iY_i)\prod_{r=0}^{p-1} Z_r \quad \textit{and} \tag{27}$$

$$a_p^\dagger = Q_p^\dagger \prod_{r=0}^{p-1} Z_r = \frac{1}{2}(X_i iY_i)\prod_{r=0}^{p-1} Z_r \tag{28}$$

where $Q_p = \frac{1}{2}(X_i + iY_i)$ and $Q_p^\dagger = \frac{1}{2}(X_i iY_i)$ are the qubit creation and annihilation operators respectively, and X, Y and Z are Pauli matrices. Using these formulas, a single fermionic excitation can be re-expressed using quantum gate operators:

$$U_p^k(\theta) = e^{-i\frac{\theta}{2}(X_pY_k - Y_pX_k)\prod_{r=p+1}^{k-1} Z_r} \tag{29}$$

Such an exponential of Pauli matrices can be represented as a quantum circuit[5]. To understand the exponential map of the product of Pauli spin matrices, first consider the exponential map of two Z operators. To create the unitary gate $e^{-i\frac{\theta}{2}(Z_0Z_1)}$, a *CNOT* gate can be used to entangle two qubits, then a R_z gate is applied, and followed by a second *CNOT* gate [see in a simulator]:

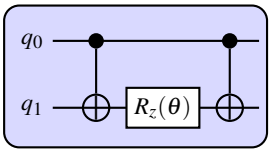

In the context of excitation circuits, every qubit represents the occupancy of a spin orbital in a chosen basis set. This construction can be generalized to more qubits (orbitals) by using additional *CNOT* gates. The formula $e^{-i\frac{\theta}{2}(Z_pZ_q...Z_kZ_l)}$ is simulated by the following quantum circuit:

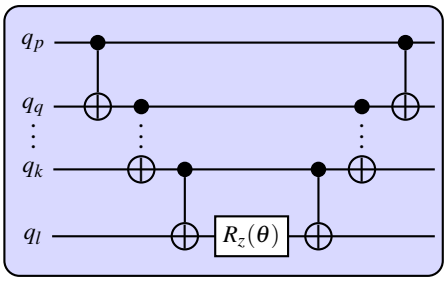

If one requires a different tensor product of Pauli matrices besides the product of Z matrices, a change of basis can be accomplished by using the appropriate unitary transformation. Hadamard transformation changes between X and Z basis, and $R_x(\frac{\pi}{2})$ transforms basis Y to Z. Afterwards gates H and $R_x(-\frac{\pi}{2})$ are used to switch the qubits back to basis Z. [see in a simulator] Based on this, the single fermionic excitation from orbital p to orbital k, denoted by $U_p^k(\theta) = e^{-i\frac{\theta}{2}(X_pY_k - Y_pX_k)\prod_{r=p+1}^{k-1} Z_r}$ can be represented in a quantum circuit. The full circuit is presented in the appendix fig. 6 [see in a simulator]

The formula for a double fermionic excitation is of the form [see in a simulator]:

$$U_{pq}^{kl}(\theta) = exp(-i\frac{\theta}{8}(X_pX_qY_kX_l + X_pX_qX_kY_l + X_pY_qY_kY_l$$
$$+ Y_pX_qY_kY_l - X_pY_qX_kX_l - Y_pX_qX_kX_l \quad (30)$$
$$- Y_pY_qX_kY_l - Y_pY_qY_kX_l) \prod_{r=q+1}^{p-1} Z_r \prod_{r'=l+1}^{k-1} Z_{r'})$$

The first term in this formula:

$$exp(-i\frac{\theta}{8}(X_pX_qY_kX_l + \ldots) \prod_{r=q+1}^{p-1} Z_r \prod_{r'=l+1}^{k-1} Z_{r'}) \quad (31)$$

is implemented in a quantum circuit as such:

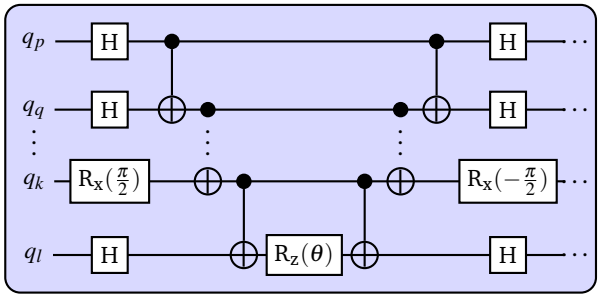

This outline presents the standard way of creating excitation gates in quantum circuits, however alternative approaches which compress these circuits exist. Compressed circuits[4] make the resulting ansätze more efficient computationally, as they limit the amount of quantum gate operators used.

The complete UCC ansatz can be constructed by adding all excitations to a circuit containing a Hartree-Fock reference state, which can be added to a quantum circuit using *NOT* gates. By default all qubits in a quantum circuit are initialized in state $|0\rangle$, using *NOT* gates essentially sets desired qubits to $|1\rangle$. For H_2 the reference state is of the form [see in a simulator]:

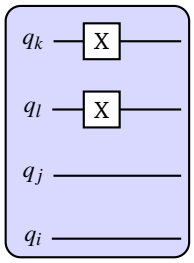

2.4 Variational Approach To Estimating Energies on a Quantum Computer

The Variational Quantum Eigensolver (VQE)[6,1] was proposed as a method to find approximate ground states of molecular Hamiltonians with near-term quantum hardware (current generation of quantum computing devices that have a limited number of qubits and shorter coherence times) in mind. It is based on the Hybrid Quantum Classical (HQC) approach, wherein one uses quantum resources in tandem with classical computers in order to exploit the available quantum resources to the utmost extent while outsourcing the optimisation task to a classical machine. VQE uses the quantum computer for state preparation using a parameterized unitary operation $U(\theta)$ (the ansatz), and the estimation of the expectation value of an observable $\hat{H}$ The expectation value is then minimised as per the variational principle using a classical optimisation algorithm. The parameters of the unitary operator are optimised iteratively until convergence in the energy. The whole process can be summarised as:

$$E_{\min} = \min_{\theta} \langle \hat{H} \rangle_{U(\theta)}, \quad (32)$$

$$\langle \hat{H} \rangle_{U(\theta)} \equiv \langle 0|U^{\dagger}(\theta)\hat{H}U(\theta)|0\rangle \quad (33)$$

A visual overview of the process is presented in fig. 3.

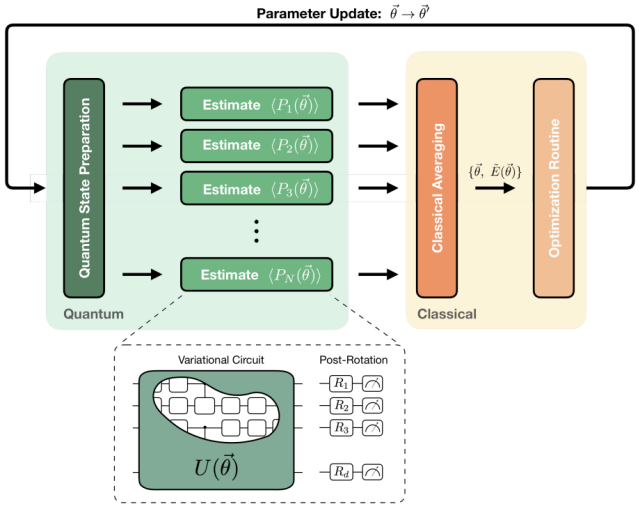

Fig. 3 Taken from:[7]; Illustration of the VQE algorithm. the quantum computer is used to prepare a set of parametrized quantum states followed by applications of rotations R_i. The classical computer then takes the individual estimates of the Pauli term expectation values $< P_i(\vec{\theta}) >$ and averages them to compute a single value $\bar{E}(\vec{\theta})$. This cost function value is fed into an optimization routine, which produces an updated set of parameters $\vec{\theta}$ as input for the quantum circuit in the next optimization loop. This procedure is repeated until the energy converges.

Using the optimal parameter values $\theta^* \equiv \text{argmin}_{\theta}\langle \hat{H} \rangle_{U(\theta)}$, one can write the ground state of the system as $|\Psi\rangle = U(\theta^*)|0\rangle$. When using a UCC-type ansatz the HF reference state has to be contained in $U(\theta)$.

2.5 The k-UpCCGSD Ansatz

The k-UpCCGSD (k Pair Unitary Coupled Cluster with Generalized Singles and Doubles) ansatz introduced in "Generalized Unitary Coupled Cluster Wavefunctions for Quantum Computation"[8] encorporates aspects of multiple CC variations as a way of obtaining an accurate and computationally efficient ansatz.

In Generalized CC (GCC) the single and double excitation terms do not distinguish between occupied and unoccupied orbitals, and are therefore referred to as generalized singles and

doubles (GSD). As a result CCGSD allows for excitations from occupied to virtual orbitals, as well as excitations from occupied to occupied ones, which yields a more accurate and robust ansatz when compared to the simpler UCCSD.

pCCD[9], also known as Ap1roG[10] is a variation on CC which a very limited number of doubles amplitudes, namely it contains only the two body excitations that move a pair of electrons from one spatial orbital to another:

$$\hat{T}_2 = \sum_{ia} t_{i_\alpha i_\beta}^{a_\alpha a_\beta} \hat{a}_{a_\alpha}^\dagger \hat{a}_{a_\beta}^\dagger \hat{a}_{i_\beta} \hat{a}_{i_\alpha} \tag{34}$$

where the summation runs over occupied and unoccupied spatial orbitals.

Despite being much simpler than spin-restricted CCSD (RCCSD) pCCD is less prone to a non-variational failure when breaking bonds.

The k-UpCCGSD model uses generalized singles and pair Doubles, and takes a product of a total of k unitary operators to increase the flexibility of the wavefunction. For a chosen integer k, k-UpCCGSD is defined as:

$$|\Psi\rangle = \prod_{\alpha=1}^{k} (e^{\hat{T}^{(\alpha)} - \hat{T}^{(\alpha)\dagger}}) |\Phi_{\text{ref}}\rangle \tag{35}$$

where each $\hat{T}^{(\alpha)}$ contains its own independent set of variational parameters θ. Because the doubles term in k-UpCCGSD is so limited when compared to standard UCCSD, its circuit depth is greatly decreased and scales linearly with system size, with a prefactor that is increased by a factor of k.

2.6 Summary of the Quantum UCC procedure

To create the UCC ansatz and optimize the θ parameters in a VQE procedure, these steps can be followed:

- Defining the molecular system of interest by providing the atoms, their coordinates and the basis set.
- Mapping the electronic structure problem onto a quantum circuit using transforms such as Jordan-Wigner.
- Constructing the UCC ansatz.
- Defining the objective function (the expectation value of the Hamiltonian operator with respect to the UCC ansatz).
- choosing an optimization algorithm such as VQE.
- (optionally choosing a backend for simulating quantum hardware)
- Performing the VQE optimization to find the optimal parameters (fig. 3).
- Computing the final energy.

3 Methodology

The UCC ansätze evaluated in ensuing parts of this outline were constructed in python using the qiskit library for working with quantum computers. The VQE algorithm was likewise sourced from qiskit. The orbitals represented in quantum circuits by qubits were obtained using the STO-3G basis set, as it is a minimalistic molecular system that can be easily represented using a small number of qubits. Moreover STO-3G can be used as a standardized benchmark, making it possible for different research groups and quantum computing platforms to compare their results and methodologies on a common test case. Likewise the FCI, classical CC, and HF calculations, which quantum UCC calculations were compared to, were also performed using the STO-3G basis set. It's worth noting that qiskit by default associates the qubits in generated circuits first with alpha orbitals, followed by beta orbitals. This has to be kept in mind while constructing ansätze, as some circuits may at face value appear different then the ones presented in this outline. The dissociation curve calculated using a noisy backend simulation was generated using tequila, as it provides a much more flexible environment for chemical computations when compared to qiskit.

4 Results and discussion

fig. 4 presents the dissociation curve of H_2 obtained on an ideal quantum backend (no noise) using quantum UCCS and pUCCD ansätze with classical pCCD, HF, and FCI references. UCCS matches the energies obtained from HF, which means that UCCS relies on the HF reference state embedded within the ansatz. On the other hand UpCCD is able to match FCI and classical pCCD results.

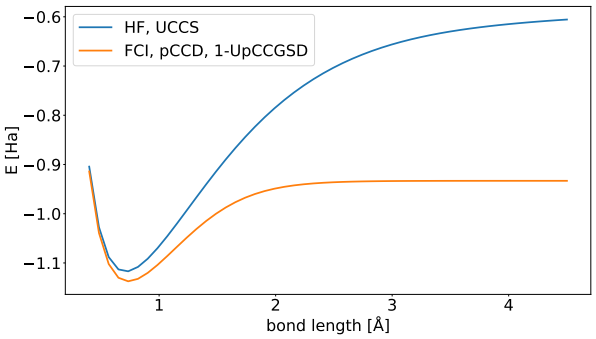

Fig. 4 Dissociation curve of H_2 for FCI, HF and classical pCCD, as well as UCCS, UpCCD evaluated on an ideal noise-free backend.

However current quantum computers are far from ideal devices, fig. 5 presents a more accurate representation of current quantum hardware capabilities. The simulator used in this calculation was the "Rome" device simulator from qiskit, a 5 qubit simulation backend that emulates the behavior of a quantum device known as the IBM Quantum Rome. The Rome device simulator in qiskit aims to mimic the noise and error characteristics of

the IBM Quantum Rome device, including features such as gate errors, measurement errors, and various noise sources that are present in real quantum hardware.

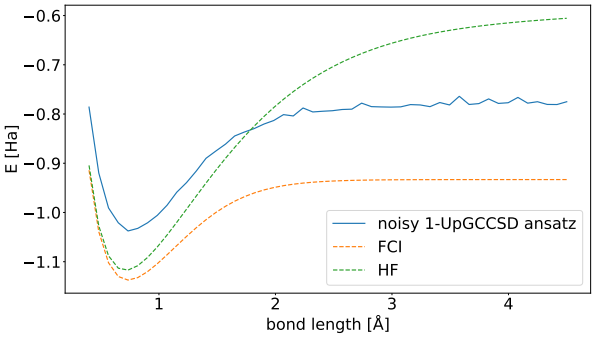

Fig. 5 Dissociation curve of H_2 for FCI, HF, and UpCCD evaluated on a noisy backend.

5 Conclusions

In theory, integrating quantum computing with an already powerful method such as Coupled Cluster has the potential to open up a number of new avenues within the field of quantum chemistry, and greatly enhance our capabilities to model molecular systems. However, this prospect is held back by the current state of quantum hardware, which to this day remains in a rather rudimentary stage of development. Modern quantum computers are unreliable and don't offer any significant advantages over their classical counterparts. Because of this the future of quantum implementations of Unitary Coupled Cluster remains closely tied to any potential advancements made in the realm of quantum computing. However, even with the current hardware limitations, there is still an incentive to improve both the theoretical and practical accuracy and efficiency of quantum UCC ansätze.

Appendix

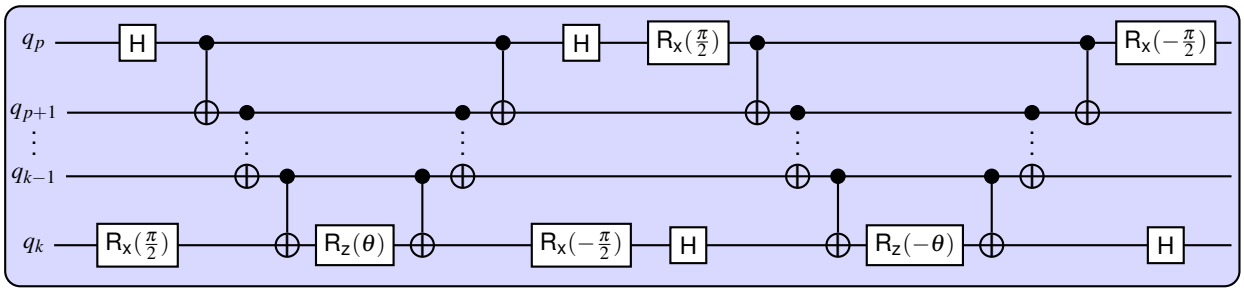

Fig. 6 The full circuit for a single fermionic excitation denoted by: $U_p^k(\boldsymbol{\theta}) = e^{-i\frac{\theta}{2}(X_pY_k - Y_pX_k)\prod_{r=p+1}^{k-1} Z_r}$.

Notes and references

1 A. Anand, P. Schleich, S. Alperin-Lea, P. W. Jensen, S. Sim, M. Díaz-Tinoco, J. S. Kottmann, M. Degroote, A. F. Izmaylov, and A. Aspuru-Guzik, "A quantum computing view on unitary coupled cluster theory," (2022).

2 R. J. Bartlett and M. Musiał, Reviews of Modern Physics **79** (2007), 10.1103/RevModPhys.79.291.

3 R. P. d. Silva, SSRN Electronic Journal (2023), 10.2139/ssrn.4347584.

4 Y. S. Yordanov, D. R. Arvidsson-Shukur, and C. H. Barnes, Physical Review A **102** (2020), 10.1103/PhysRevA.102.062612.

5 J. D. Whitfield, J. Biamonte, and A. Aspuru-Guzik, Molecular Physics **109** (2011), 10.1080/00268976.2011.552441.

6 A. Peruzzo, J. McClean, P. Shadbolt, M. H. Yung, X. Q. Zhou, P. J. Love, A. Aspuru-Guzik, and J. L. O'Brien, Nature Communications **5** (2014), 10.1038/ncomms5213.

7 Y. Cao, J. Romero, J. P. Olson, M. Degroote, P. D. Johnson, M. Kieferová, I. D. Kivlichan, T. Menke, B. Peropadre, N. P. Sawaya, S. Sim, L. Veis, and A. Aspuru-Guzik, "Quantum chemistry in the age of quantum computing," (2019).

8 J. Lee, W. J. Huggins, M. Head-Gordon, and K. B. Whaley, Journal of Chemical Theory and Computation **15** (2019), 10.1021/acs.jctc.8b01004.

9 T. Stein, T. M. Henderson, and G. E. Scuseria, Journal of Chemical Physics **140** (2014), 10.1063/1.4880819.

10 P. A. Limacher, P. W. Ayers, P. A. Johnson, S. D. Baerdemacker, D. V. Neck, and P. Bultinck, Journal of Chemical Theory and Computation **9** (2013), 10.1021/ct300902c.